Near-Real-Time Damage Estimation for Buildings Based on Strong-Motion Recordings: An Application to Target Areas in Northeastern Italy

Chiara Scaini*[1], Bojana Petrovic[1], Alberto Tamaro[1], Luca Moratto[1], and Stefano Parolai[1]

Abstract

The rapid estimation of expected impacts in case of an earthquake is extremely important for emergency managers and first responders. Current near-real-time damage assessment methods rely on ground-motion estimates and exposure or fragility datasets, in some cases integrating the shaking recorded at the site (e.g., from strong-motion monitoring networks). We propose a method that estimates the expected damages on buildings based on strong-motion recordings of a seismic event. The damage assessment is based on the maximum drift (interstory) or the displacement, which is estimated by considering in a first approximation the behavior of a specific building typology as a single-degree-of-freedom oscillator. The oscillator is characterized based on the analysis of the building stock and a large number of ambient vibration measurements performed in buildings. A specific damage state occurs when the interstory drift or displacement limits available in the literature for the specific building typology are exceeded. The method, here applied to a case study in northeastern Italy, can be applied to other seismic areas worldwide to provide quick, first-level estimates of expected damages.

Introduction

Estimating expected damages in case of a seismic event is important for emergency managers and civil protection authorities. In particular, because a large fraction of casualties during earthquakes is related to building failure (So and Spence, 2013), a quick estimation of the damage of buildings is paramount to drive effective life-saving response actions. Building typologies that share similar characteristics have been defined at global, regional, and national scales (e.g., Jaiswal and Wald, 2008; Lang *et al.*, 2018; Polese *et al.*, 2019, respectively) with growing detail and complexity. Seismic impact assessment can then be performed at global (e.g., the U.S. Geological Survey model Prompt Assessment of Global Earthquakes for Response; Wald *et al.*, 2008), regional (D'Ayala *et al.*, 2010), and national scales (Silva *et al.*, 2015; Dolce *et al.*, 2019) based on exposure data and vulnerability or fragility functions developed at different spatial resolutions (e.g., Vona, 2014; Del Gaudio *et al.*, 2017; Masi *et al.*, 2019; Donà *et al.*, 2020). However, most national damage assessments are now produced at municipality scale, whereas emergency managers (e.g., civil protection, civil defense) require first-level local-scale information to implement quick response actions. To refine the damage assessment locally, the specific features of local buildings should also be identified (e.g., Pittore *et al.*, 2018) to define specific building typologies and their distribution at local scale.

During the past decades, seismic damage and risk assessment methods have evolved to use directly the ground-motion values obtained by first-level ground-motion estimates (e.g., using ShakeMaps, Wald *et al.*, 1999, 2006) that can support a first-level damage assessment shortly after the occurrence of an earthquake (Wald *et al.*, 2008). However, the reliability of the spatial distribution of shaking depends on several factors, among them the number of seismic stations used to compute the ground motion (Moratto and Saraò, 2012). Thus, given the relevance of seismic stations coverage, strong-motion seismic networks are increasingly deployed in active seismic areas worldwide (e.g., Mori *et al.*, 1998; Okada *et al.*, 2004; Espinosa-Aranda *et al.*, 2009; Gorini *et al.*, 2010; Satriano *et al.*, 2011; Wu *et al.*, 2013; Parolai *et al.*, 2017). In particular, the National Institute of Oceanography and Applied Geophysics

(OGS) manages a dense seismological network (Sistema di Monitoraggio terrestre dell'Italia Nord Orientale (SMINO); Bragato *et al.*, 2021) currently consisting of >45 seismological stations (equipped with both seismometers and strong-motion sensors) and 58 low-cost strong-motion sensors installed in 31 buildings (SentiNet network). Low-cost strong-motion sensors installed in buildings increase the number of ground-motion observations and measure the shaking at the building's bottom and top to monitor its dynamic behavior during an earthquake.

Strong-motion recordings in the study area allow the extraction of the main ground-motion parameters in near-real time and, given a building's dynamic behavior, the estimation of its expected damages (Bindi *et al.*, 2015; Parolai *et al.*, 2015). However, this requires a characterization of the building's dynamic behavior. A first approximation of the building's dynamic behavior is given by a single-degree-of-freedom (SDOF) damped oscillator and thus by the fundamental frequency and the damping (e.g., Mucciarelli and Gallipoli, 2007). Different approaches have made use of earthquake recordings, forced vibration studies, or ambient noise measurements (e.g., Bindi *et al.*, 2015; Petrovic *et al.*, 2018) to study buildings' dynamic behavior. In particular, ambient noise measurements can be used to infer the elastic response of buildings in a quick and cheap manner while giving reliable results (e.g., Gallipoli *et al.*, 2009). Nevertheless, fundamental frequencies estimated from ambient vibration measurements may be higher than the theoretical elastic frequencies used in earthquake engineering (e.g., Michel *et al.*, 2010). Both analytical (Crowley and Pinho, 2004) and experimental (Farsi and Bard, 2004; Dunand *et al.*, 2006; Gallipoli *et al.*, 2010) approaches can be used to infer simplified relations for buildings. Several authors provided period–height relations based on noise measurements on buildings of different materials (e.g., Gallipoli *et al.*, 2009; Michel *et al.*, 2010), whereas others focused on reinforced concrete (RC) buildings (Goel and Chopra, 1997; Crowley and Pinho, 2006). However, only a few specific studies are available for unreinforced masonry (URM) buildings (Bal *et al.*, 2008; Gosar, 2012) despite their strong presence in the European building stock and in other geographic areas worldwide. To increase their usability for damage assessment purposes, such relations should be derived for specific building typologies for which the experimentally defined parameters are valid.

Here, we propose a method that, based on strong-motion recordings, allows the estimation of the expected damages for specific building typologies in target areas surrounding the recording locations. In our study, we do not perform structural dynamic simulations because we are not interested in a precise reconstruction of buildings' dynamic responses. Instead, we make use of simplified models for damage assessment based on the exceedance of specific damage thresholds following the method proposed by Parolai *et al.* (2015). They estimated the accelerations at the top of every single monitored building using the recordings at the bottom as input and assuming that the buildings behave as single- or multiple-degree-of-freedom oscillators (SDOF or MDOF, respectively). Here, the method has been extended to estimate the interstory drift and displacement for selected building typologies based on the fundamental frequency obtained from experimental studies. Expected damage can be subsequently estimated by forecasting the interstory drift or displacement values and comparing them with the limits proposed in the literature for the damage state and building typology.

To show the feasibility of the damage assessment method, we apply it to five municipalities located in northeastern Italy at the border between Friuli Venezia Giulia (FVG) and Veneto regions (Fig. 1), hit by several historical earthquakes in the past 1000 yr (Rovida *et al.*, 2021). In particular, the Cansiglio earthquake (October 1936) caused substantial damages in the selected area (Guidoboni *et al.*, 2019). In case of repetition of such an event, historical masonry buildings would be strongly affected (Bernardini *et al.*, 2008; Meroni *et al.*, 2008). However, no specific damage scenarios exist for modern masonry buildings constructed after that event that belong to a common building typology in northeastern Italy. Within the five selected municipalities, we identify target areas where the considered building typology is present and estimate the expected damage for the historical event of 1936 Cansiglio. Results allow to produce a first-level estimate of the expected damage on the considered building typology in populated areas in the proximity of the locations where broadband seismograms were simulated.

Methodology

Prerequisites

The proposed method for the estimation of expected damages in a target area relies on the following information:

- Knowledge about the existing building typologies and their distribution in the target area. The target area is defined as an area where the event is recorded and where the intensity of ground motion can be considered homogeneous. The size of the target area depends on many factors, in particular on the heterogeneity of the soil conditions and the resolution of exposure data. The size may vary for different sites.
- Fundamental frequencies of the considered building typologies, estimated either from experimental studies or from period–height relations.
- Recording of an earthquake in the target area.

Calculation of the acceleration at the top of a building

Parolai *et al.* (2015) have shown that the acceleration at the top of a building can be estimated as a sum of the relative acceleration calculated using the Z-transform (e.g., Lee, 1990; Jin *et al.*, 2004) from the recording of a single instrument installed at the basement of the building and this recording at the

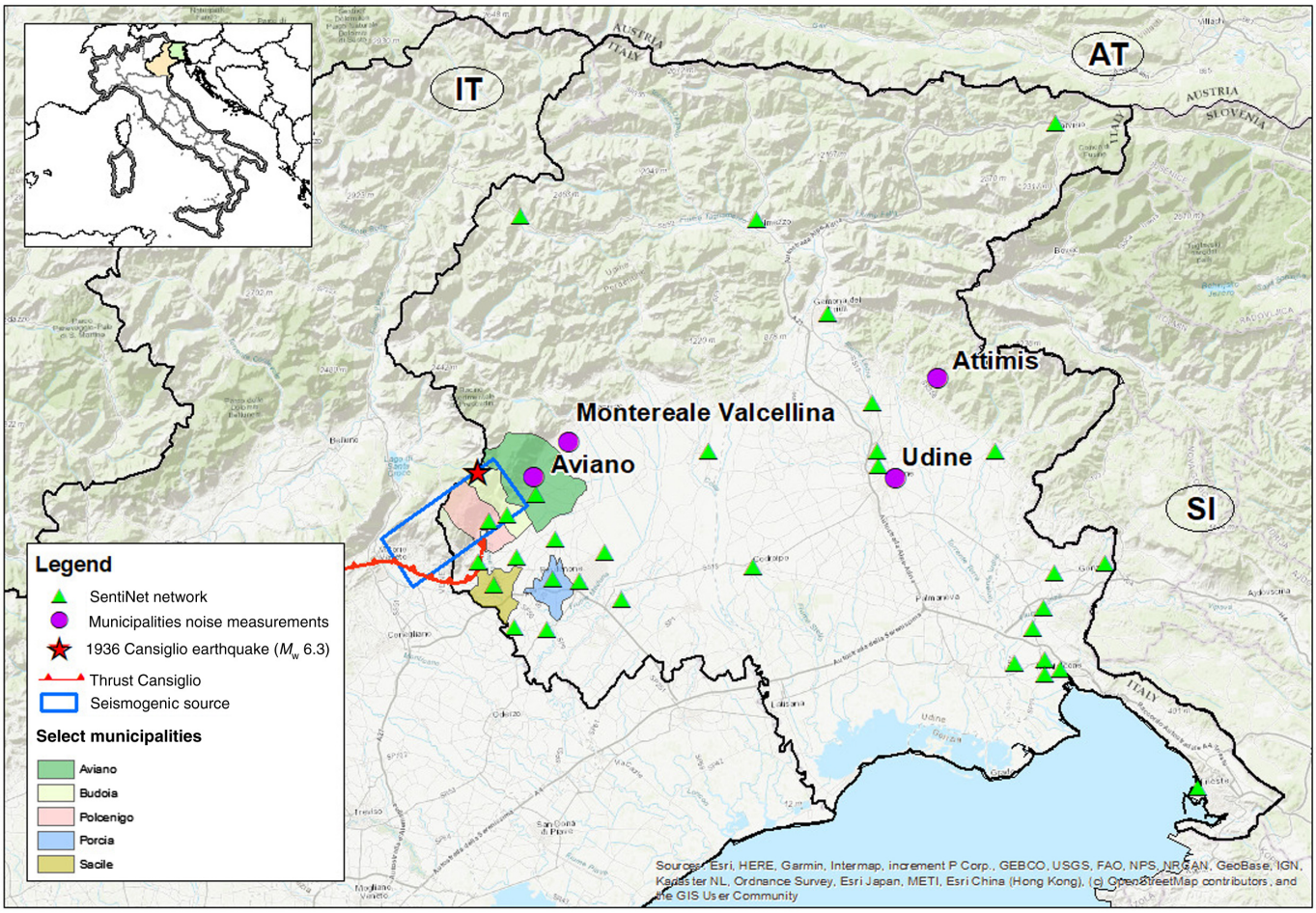

Figure 1. Map showing the 1936 Cansiglio epicenter (star) with its finite-fault area (blue rectangle), the seismological network (National Institute of Oceanography and Applied Geophysics network), the network of instrumented buildings (SentiNet, up-to-date to November 2020), the selected municipalities (Aviano, Budoia, Sacile, Polcenigo, and Porcia), and the municipalities where noise measurements were performed (Aviano, Montereale Valcellina, Attimis, and Udine). The top-left inset shows the location of the study area in northeastern Italy. The area is located at the border between FVG and Veneto regions, highlighted in color. The color version of this figure is available only in the electronic edition.

basement. The buildings were assumed to behave as SDOF or MDOF oscillators, depending on the complexity of the considered building. For simple built structures, for which the fundamental translational mode is dominant and thus provides the main contribution to the vibration of the building (usually buildings with 1–5 stories), the building's behavior can be simulated as those of an SDOF oscillator (e.g., Lee, 1990). For more complex structures, an MDOF oscillator has to be considered. Parolai *et al.* (2015) proposed to perform the simulation for MDOF oscillators considering the contribution of the main vibrational modes and weighting them, in a first-order approximation, by calculating their contribution based on the spectral peak amplitudes in the Fourier amplitude spectra at the top of the building.

Estimation of the displacement and the interstory drift ratio

The relative displacement (drift) at the top of a building can be calculated in the same way from the recording at the basement of the building with the Z-transform (e.g., Jin *et al.*, 2004) by simulating the behavior of a building by an SDOF or MDOF oscillator with the natural frequency ω_0 and the damping ratio ζ. The drift $x(t)$ due to an input recording a_{j-1} can be recursively calculated as follows:

$$x_j = b_1 x_{j-1} + b_2 x_{j-2} - S_0(\Delta t)^2 a_{j-1}, \tag{1}$$

with the coefficients b_1, b_2, and S_0 defined as

$$b_1 = 2e^{-\zeta\omega_0\Delta t}\cos(\omega_d\Delta t), \tag{2}$$

$$b_2 = -e^{-2\zeta\omega_0\Delta t},$$

$$S_0 = e^{-\zeta\omega_0\Delta t}\sin\frac{(\omega_d\Delta t)}{(\omega_d\Delta t)},$$

$$\omega_d = \omega_0(1-\zeta^2)^{\frac{1}{2}}.$$

The displacement at the top of the building is obtained as the sum of the calculated drift (equation 1) and the displacement at the bottom of the building. The latter is calculated by double integration of the acceleration recorded at the bottom of the building over time. The total displacement and interstory drift are calculated for both directions (main building axes) by the equivalent SDOF or MDOF oscillators, and the maximum of both directions is considered.

From single buildings to building typologies

The work of Parolai *et al.* (2015) leads to the estimation of the acceleration at the top of a single building. Here, we focus on the estimation of the displacement and extend the method from single buildings to building typologies. Different building typologies are characterized by many factors, the most relevant being age, construction material and height, and can be defined based on the analysis of the building stock in the area of interest. We assume that buildings belonging to the same typology have a similar linear dynamic response. Thus, their response to a seismic input can be approximated by a single, representative SDOF or MDOF oscillator for which the fundamental frequency and damping value are selected based on experimental data or existing relations (e.g., from Eurocode 8, CEN, 2004).

Determination of the expected damage for building typologies

Applying the method described previously, the maximum expected displacement and drift values can be calculated for a certain building typology.

Nonstructural damage: This estimation is based on the comparison of calculated maximum total or interstory drift (drift divided by height of the building) and threshold values proposed by the building codes. If the calculated maximum drift is greater than the limits, the occurrence of nonstructural damage is expected. For Europe, threshold limits are provided by the Eurocode 8 (CEN, 2004). In addition, the Italian national building code provides specific values for different building typologies (Norme Tecniche per le Costruzioni [NTC], 2018).

Structural damage: This estimation is based on the comparison between the calculated maximum total displacement at the top of the building and the displacement thresholds available in the literature for different building typologies and structural damage states. For Europe, Lagomarsino and Giovinazzi (2006) defined displacement thresholds for the most common building typologies, including several RC and masonry types. Similarly, other studies provide interstory drift limits for specific building typologies and/or geographic areas (e.g., Ruiz-Garcia and Negrete, 2009). Other references are available in the literature for different countries and geographic regions, for example, Greece (Penelis *et al.*, 2003), Canada (Abo-El-Ezz *et al.*, 2013), the United States (Frankie *et al.*, 2013), Mexico and Latin America (Ruiz-Garcia and Negrete, 2009), India (Chourasia *et al.*, 2016), and Pakistan (Shahzada *et al.*, 2012).

Expected damage in the target area

Based on the number and distribution of the buildings that belong to the considered typologies, it is possible to calculate the number of buildings that are expected to sustain nonstructural and structural damages in the target area. An example of the total damage estimation in the target areas is provided for the test site.

Test Site

We selected five municipalities in FVG (Fig. 1), in which strong-motion sensors were installed on target buildings (SentiNet network, Bragato *et al.*, 2021). The municipalities that sustained the largest damages during the 1936 Cansiglio event (M_w 6.3 according to Sirovich and Pettenati, 2004) were selected. The recorded macroseismic intensities were 7 in Porcia and Aviano, 7–8 in Sacile, and 8 in Budoia and Polcenigoand (Rovida *et al.*, 2021). Figure 1 shows the OGS monitoring networks (up to date to November 2020), the selected municipalities, and the areas where noise measurements and inspections have been performed on residential buildings.

Collected data

To apply the method to the case study, we use the following data available for the study area.

Information on building typologies and their distribution in the target area:

- 2011 census data provided by the Italian National Institute of Statistics (Istat, 2011). The 2011 census is the last complete census in Italy and contains building age, number of stories, and material. Building data, publicly available at municipality level, were provided by Istat at the census units level for the purpose of this study.
- Digital building map for the FVG region (Carta Tecnica Regionale Numerica 1:5000; see Data and Resources) that contains the buildings' usage, area, and height, inferred from photogrammetric analyses.
- Information from local inspections, interviews with municipality technicians and practitioners, and analysis of the municipality master plans. This information was collected both inside and outside the target areas.

Fundamental frequency for the selected building typology:

- Ambient vibration measurements performed simultaneously inside and outside the target area in 22 buildings of the same building typology.

Because no damaging earthquake occurred recently in the studied area and no recordings of strong events are available, we simulate broadband near field recordings for the 1936 Cansiglio earthquake. The synthetic seismograms are simulated in the location of the instrumented buildings for the five selected municipalities.

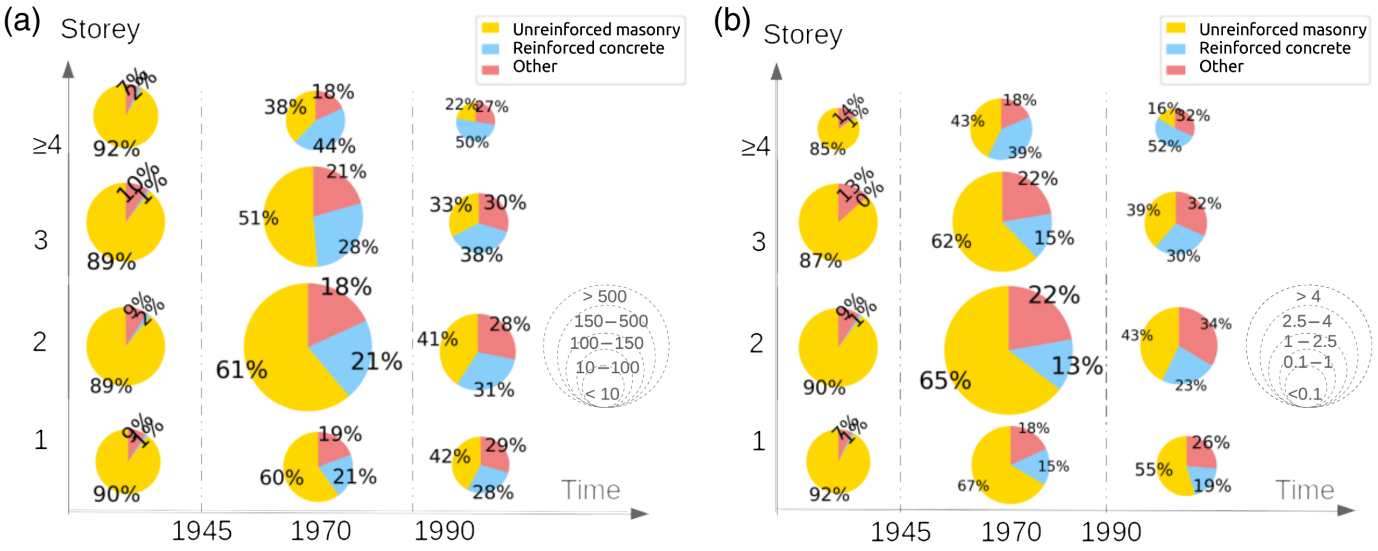

Figure 2. Summary of the building stock according to the Istat Census 2011 for (a) Friuli Venezia Giulia (FVG) and Veneto regions (~1.3 million buildings in total) and (b) the selected municipalities (~15, 000 buildings). Sizes of pie charts are proportional to the number of buildings according to the graphical legend (units are thousands of buildings). The uppermost height class contains all buildings that have four or more stories. The color version of this figure is available only in the electronic edition.

Building typologies in northeastern Italy

The definition of the building typology considered in this work is based on the classification of the Italian 2011 Census (Istat, 2011). The analysis of Istat data shows that a high percentage of the building stock in FVG and Veneto consists of URM constructed in the period 1946–1990 (Fig. 2a). The same analysis for the selected municipalities shows that the building stock follows the same pattern and can be thus considered representative for northeastern Italy (Fig. 2b).

Building inspections were performed for 54 buildings in four municipalities inside and outside the target area (Fig. 1) to identify the main features of the selected typology (Fig. 3a), mostly consisting of concrete blocks (Fig. 3b) or bricks and rigid floors and roofs (Fig. 3c), which in some cases have been originally built (Fig. 3d) or reconstructed in the 1990s using wood. Given the high presence of "other" material in the Istat database that, for northeastern Italy, is normally a combination of URM and RC elements (e.g., local reinforcements), we include buildings constructed of "other" material into the identified masonry building typology.

Thus, the selected building typology for this case study is URM buildings (in some cases, in combination with RC elements), consisting of concrete blocks or construction material classified as "other," built in the period 1946–1990. Such buildings account for a high fraction of postwar residential buildings in northeastern Italy (Ferrario, 2009). We focus our study on regular and stand-alone buildings belonging to the considered building typology because their dynamic response can be modeled with an SDOF equivalent oscillator. In this work, we propose a method to automatically extract the following indicators from the digital building map, using a Geographic Information System (GIS) engine:

- **Number of stand-alone buildings:** Each building in the digital building map corresponds to a single polygon, with the exception of multiple housing units (e.g., terraced or row houses). We consider map polygons as stand-alone buildings when (a) they have no neighbors and (b) the perimeters are lower than 120 m. This value has been selected based on the analysis of stand-alone buildings' perimeters in the study area. In the opposite case, they are considered as attached buildings.
- **Number of buildings in each height class** (Fig. 4b): The digital building map contains building footprints and their associated eave height, which has been converted into an equivalent number of stories (see legend of Fig. 4b).
- **Number of buildings regular in plan** (Fig. 4c): According to the Italian building code (NTC, 2018), buildings considered "regular in plan" should have a shape ratio (i.e., the ratio between long and short edges of the minimum bounding rectangle of the building) lower than 4. To comply with the NTC additional requirements on building shape irregularity, as a precaution we reduce the shape ratio limit for regular buildings to 2. Other building codes provide different criteria to distinguish between buildings that are regular and nonregular in plan, and the methodology can be adapted accordingly.

The automated procedure described previously identifies the regular and stand-alone buildings in a specific area but introduces a degree of uncertainty in the results. There are, in fact, discrepancies between the number of buildings in the national

Figure 3. (a) An example of a three-story masonry building belonging to the considered typology and the details of (b) blocks constituting the load-bearing vertical structure, (c) rigid roof, and (d) pre-existent wooden roof. The color version of this figure is available only in the electronic edition.

building census and digital building maps (Gallipoli *et al.*, 2020) and their characteristics (Bernardini, 2008). In addition, the simplified method to identify regular buildings from the buildings' footprint only accounts for the regularity in plan but not for the distribution of mass and stiffness (for which specific criteria exist in most building codes). For the target areas considered in this work, visual inspection confirmed the regularity in shape of the single houses, typical of the Italian postwar urbanization. Moreover, the number of buildings in each story class of the Istat database is in most cases comparable with the number of buildings in the digital building map in each height interval. Further work is nevertheless required to validate and generalize the approach.

Characterization of target areas

For each of the five municipalities, we define the target area by selecting the census units that intersect an 800-m-radius circular area centered around the location of the simulated ground motion (i.e., the location of the SentiNet building). The radius for this test site has been defined based on the analysis of the soil maps in the target areas, homogeneous in the surrounding of the simulated ground-motion location, where no significant variation of the site amplification is expected. We consider only the census units in which at least 50% of buildings belong to the selected typology and discard those that contain less than 20 buildings (to obtain robust results in statistical sense). Figure 4a shows as an example the circular area and the census units for Aviano. Figure 4b,c shows the height distribution and the buildings shape ratio for one of the census areas in the municipality of Aviano.

It is then possible to calculate the percentage of regular and stand-alone buildings for each height interval and apply this percentage to the number of buildings that, according to the Istat database, belong to the chosen typology (i.e., URM buildings, consisting of concrete blocks or construction material classified as "other," built in the period 1946–1990). The calculation is performed for each census unit, and the totals are calculated for the target areas of the five selected municipalities (Table 1). All target areas have a high percentage of buildings that belong to the typology. The lower percentages of regular and stand-alone buildings in Budoia and Polcenigo are due to the higher irregularity of building footprints and the higher discrepancies between census data and digital building map. The buildings that belong to the typology in the target area are 1763, of which 954 are regular and stand alone.

Experimental estimation of fundamental frequency

Seismic noise measurements were carried out in 22 masonry buildings of two, three, or four stories, constructed between 1946 and 1990 with bricks or blocks and having rigid floors. Because this building construction type is very common in the

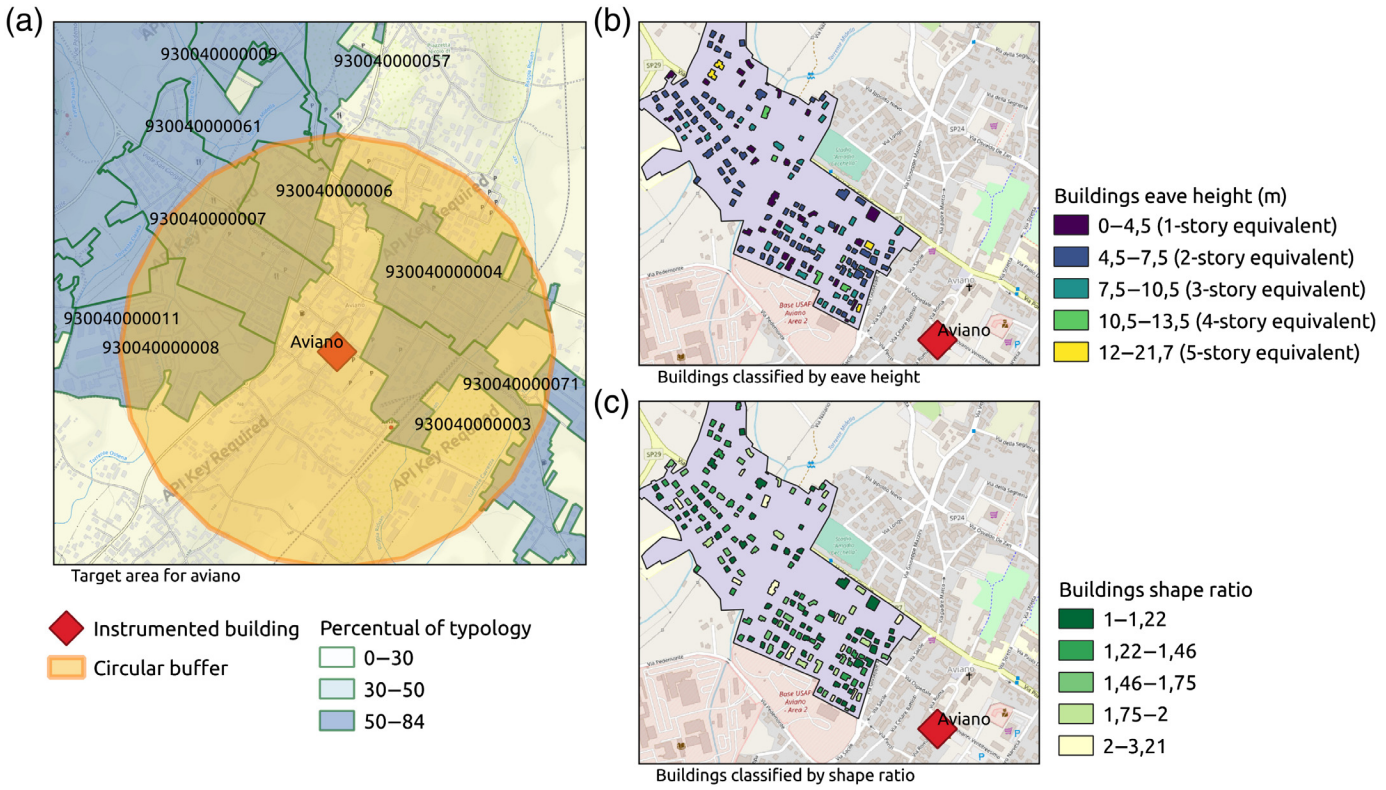

Figure 4. Example of target area characterization for the municipality of Aviano. (a) Circular area and selected census units that constitute the target area for Aviano. (b) Example of buildings height classification for one of the census unit in the target area. (c) Example of shape ratio classification for stand-alone buildings identified within the census unit in the target area. The color version of this figure is available only in the electronic edition.

whole FVG region, measurements were performed in four municipalities located inside and outside the target areas: Aviano, Montereale Valcellina, Attimis, and Udine (Fig. 1). The buildings were selected by two criteria: (a) selected building typology and (b) permission of the residents to carry out measurements. The seismic noise measurements of 30 min were performed at the top and the bottom of each building, assuming the later one to represent a free-field measurement. For the two horizontal and the vertical directions, the Fourier amplitude spectra are calculated using a moving window of ~1 min, overlapping by 50% and cosine tapering at both ends. Subsequently, the average spectra are estimated and the fundamental frequency for each building is calculated.

In Figure 5, the period T of the 22 analyzed masonry low-rise buildings is plotted versus the height H of the buildings (black dots). From a simple linear regression (black line, Fig. 5), we obtain

TABLE 1
Total Number of Buildings in Each Municipality's Target Area, Percentage of Buildings That Belong to the Considered Building Typology, and Percentage and Number of Those That Are Regular and Stand-Alone

Municipality	Total Number of Buildings in Target Area	Buildings That Belong to the Typology (%)	Regular and Stand-Alone Buildings That Belong to the Typology (%)	Number of Regular and Stand-Alone Buildings That Belong to the Typology
Aviano	434	71%	47%	202
Budoia	129	54%	26%	33
Polcenigo	465	78%	19%	88
Sacile	510	74%	43%	218
Porcia	893	72%	46%	413

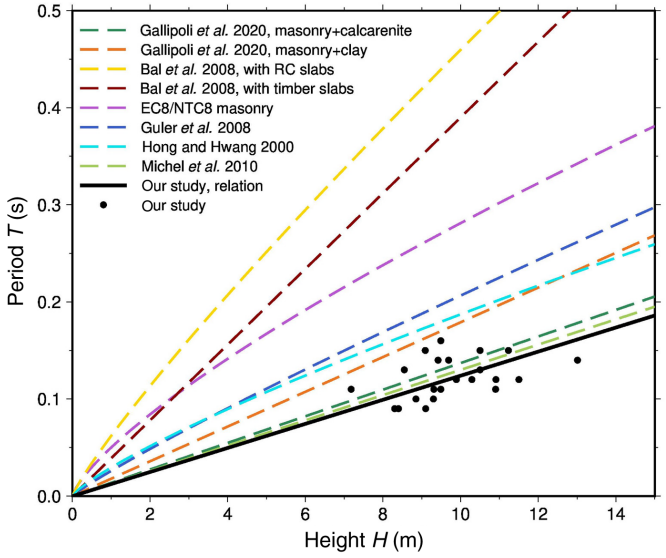

Figure 5. Comparison of our *T*–*H* relation obtained for masonry buildings in FVG (results for single buildings are also shown) with relations from other studies of both RC and masonry buildings. The color version of this figure is available only in the electronic edition.

$$T = 0.0124H. \quad (3)$$

Our results are compared with *T*–*H* relations provided by other authors. It is striking that especially the relations estimated by Bal *et al.* (2008, based on nonlinear dynamic analyses) for masonry buildings with RC slabs (yellow dashed line) and with timber slabs (red dashed line) in Turkey overestimate considerably our results. Furthermore, the periods provided by the earthquake design code for masonry buildings (EC8 and NTC8, violet dashed line) are significantly larger than the periods obtained from the ambient vibration recordings. Some other studies, based on noise measurements, fit them better. For example, Hong and Hwang (2000, cyan dashed line) and Guler *et al.* (2008, blue dashed line), mainly focused on RC buildings, fit our relations but with an overestimation. A relation derived by Michel *et al.* 2010 (light green dashed line) for French buildings, including both RC and masonry buildings, fits well our results. A recent study of Gallipoli *et al.* (2020) focused on the evaluation of the soil-building effect in Matera. Our results are also compared with their relations obtained for masonry buildings on clay (orange dashed line) and calcarenite (dark green dashed line, personal comm.). Our *T*–*H* relation for masonry buildings in FVG is close to their relation for masonry buildings on calcarenite soil. The discrepancies between our relations and the ones of the other authors may be caused by different soil conditions, different building typologies, or a combination of both.

Validation of Drift and Displacement Estimation with Weak-Motion Data

Until now the SentiNet network did not register any close strong-motion events. For the validation of the drift and total displacement estimation, the approach is applied to recordings of an M_L 3.7 event that occurred in Tramonti di Sopra on 13 July 2020 (see Data and Resources) and was registered by the SentiNet sensors installed in the Aviano city hall at 30 km distance. The three-story masonry building is monitored by two sensors, one installed at the top and one at the bottom of the building; the sensors are oriented along the main building axes. The building has been simulated to behave as an SDOF oscillator in both horizontal directions, with fundamental frequencies of $f_x = 6.7$ Hz and $f_y = 7.6$ Hz and a damping factor of 10% and 5% for the x and y directions, respectively. The fundamental frequencies have been estimated from seismic noise measurements at different points in the building, the damping factors as those fitting best the recordings at the top. A more detailed and specifically dedicated study of the damping factor in low-rise masonry buildings will be performed in the future. In Figure 6, the total simulated displacement and the total displacement at the top obtained by a double integration of the acceleration recorded at the top are shown for both directions (left: x direction, right: y direction). The simulated total displacement is calculated as a sum of the displacement at the bottom, obtained by a double integration of the acceleration registered at the bottom and the simulated drift calculated with equation (1). For comparison, also the drift estimated as the difference of the displacement at the top and the bottom is shown in Figure 6e. For both directions, the simulated displacements (Fig. 6a) show a high correlation (correlation coefficient between 0.8 and 0.9) with the displacements obtained from the recordings (Fig. 6b). The maximum simulated total displacement differs from the maximum total displacement from the recordings by 6% and 9% for the x and y directions, respectively. Here, we demonstrate for a building that it is possible to reconstruct the recordings at the top (and in particular the displacement) from those at the bottom in a satisfactory way. For our method, the precise reconstruction of the recordings is out of scope, but we are interested in the maxima of total displacement and drift and its exceedance in case of strong events. The deviation of the determined value from the measured maximum is negligible. The maximum total displacement (below 0.0001 m for both directions) and interstory drift are below the limits for which structural or nonstructural damage is expected.

Simulation of the 1936 Cansiglio Earthquake

The Cansiglio earthquake (18 October 1936) was one of the stronger seismic events that occurred in the twentieth century in northeastern Italy and caused severe damages and fatalities in a wide area located at the border between Veneto and FVG regions (Fig. 1).

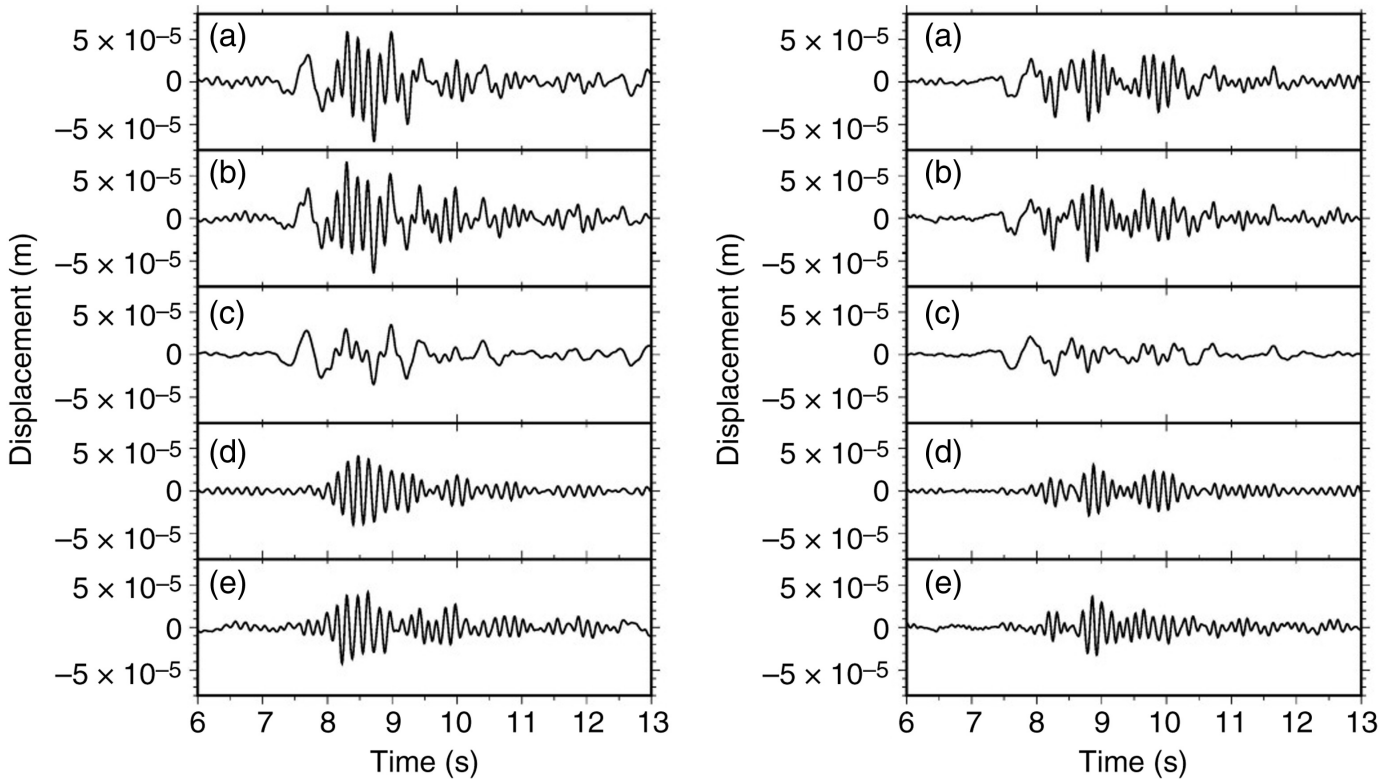

Figure 6. (a) Simulated displacement at the top of the building. (b) Displacement at the top of the building obtained by double integration of the acceleration recording. (c) Displacement at the bottom of the building obtained by double integration of the acceleration recording. (d) Simulated drift using Z-transform. (e) Drift calculated as difference of displacement at top and bottom. Left panels denote *x* direction and right panels denote *y* direction.

The broadband seismograms related to this earthquake are simulated using a hybrid approach (Moratto *et al.*, 2015) that merges low-frequency deterministic signals (Spudich and Xu, 2003) with the high-frequency stochastic part (Motazedian and Atkinson, 2005). The finite-fault parameters are taken from Sirovich and Pettenati (2004) who inverted the macroseismic observations: the released seismic moment is 3.23×10^{25} dyn · cm ($M_w = 6.3$) with a fault length of 19.6 km; the rupture started at a depth of 15.3 km and propagated principally toward southwest (Fig. 1). The associated slip distribution has one asperity (Moratto *et al.*, 2011) and was used as input in the pseudodynamic approach (Guatteri *et al.*, 2004), which reproduces the dynamic features of the rupture. In the low-frequency calculation, we use the velocity structure model by Moratto *et al.* (2012), specific for the studied area, whereas the stochastic computation adopts the propagation parameters estimated by Malagnini *et al.* (2002) for northeastern Italy. We estimate the macroseismic intensity (IMS) form peak ground acceleration applying the empirical relation by Gomez-Capera *et al.* (2020): our simulations reproduce satisfactorily the intensity observed at Aviano, Budoia, and Polcenigo (Rovida *et al.*, 2021). However, the simulations underestimate the intensity associated with Porcia (6) compared with the observed ones (7). The synthetic seismograms for all three components (north, east, and vertical) and all five considered sites are shown in Figure S1 of the supplemental material available to this article.

Because a local velocity structure at all investigated sites is not known, the numerical simulations are carried out for a rock site. However, in case of strong motion, the site response might change because of nonlinearity, increasing the uncertainties in the estimation of the input motion. These assumptions might affect the input ground-motion reliability at some of the investigated sites, and this issue must be taken into account when interpreting the results.

Damage Assessment Results

Expected damage is estimated for the considered building typology using the method described earlier. Therefore, the estimated maximum displacements are compared with the limits identified in the literature for the building typology and for selected damage levels. In this study, we focus only on structural damage and consider two structural damage levels: extensive and complete. Extensive and complete structural damage levels correspond to D3 and D4–D5 of the European Macroseismic Scale (Grünthal, 1998), respectively (Lagomarsino and Giovinazzi, 2006). In particular, Lagomarsino and Giovinazzi (2006) propose a relation between damage state and yielding and ultimate displacements of the building capacity curve: extensive damage corresponds to the average between yielding

TABLE 2
Displacement Limits That Identify Extensive and Complete Structural Damage for the Considered Unreinforced Masonry (URM) Building Typology According to Lagomarsino and Giovinazzi (2006)

Damage Level	Extensive	Complete
URM low rise (1–2 stories)	0.0138 m	0.0236 m
URM mid rise (3–4 stories)	0.0219 m	0.035 m

and ultimate displacements, whereas complete damage corresponds to the ultimate displacement. Table 2 collects the displacement limits provided by Lagomarsino and Giovinazzi (2006) for European URM buildings that match the building typology considered in this study. Displacement limits at the top of such buildings are provided for two height classes, low and mid rise, which correspond to 1–2 and 3–4 stories, respectively.

The damage level is estimated by comparing the maximum displacement of the equivalent SDOF oscillator defined for the specific building typology and the aforementioned limits. The fundamental frequency of each representative SDOF oscillator is estimated using our height–period relation (equation 3) obtained from the linear regression of the experimentally estimated fundamental frequencies of 22 considered masonry buildings in the FVG region. This relation is derived by taking into account the average height of regular and stand-alone buildings in each census unit. We assume a damping factor of 5%. The seismic input is provided by the synthetic seismograms for the selected seismic event.

Damage assessment for target areas

The damage assessment procedure allows to assess the expected structural damage produced by the event of 1936 Cansiglio on the almost 1000 buildings (Table 1) that belong to the identified building typology in the target areas. Table 3 shows the estimated displacements for the building typology and the expected damage state based on the thresholds considered for the two height ranges for which the displacement limits are defined (Table 2).

Figure 7 shows the occurrence of extensive and complete damages on low- and mid-rise buildings (panels a and b, respectively) in the target areas of the five selected municipalities. For Budoia, a complete damage is expected for both low- and mid-rise buildings, whereas in Polcenigo, low- and mid-rise buildings are expected to sustain complete and extensive damage, respectively. For Aviano and Sacile, extensive damage is expected only for low-rise buildings, and no damage is expected for Porcia; thus, Porcia is not shown in Figure 7.

Discussion

Past studies (e.g., Bernardini *et al.*, 2008; Meroni *et al.*, 2008) found that in case of repetition of the 1936 Cansiglio earthquake, substantial impacts are expected in the western FVG area. The SentiNet network is particularly dense in this area, so the selected case study is realistic in case of events occurring nearby. Our results show that for the Cansiglio event, structural damage would occur in target areas for all considered municipalities except Porcia (Table 3). The totally damaged buildings represent a substantial percentage of the buildings in the target areas (between 45% and 65% in all municipalities except Polcenigo) and host altogether ~9800 inhabitants who

TABLE 3
Displacement Values and Expected Damage States for Each Municipality and for the Two Height Ranges Considered for the Building Typology

Municipality	IMS (Recorded)	IMS (Simulated)	Height Range	Displacement	Damage State
Aviano	7	7	Low rise	0.0200	Extensive
			Mid rise	0.0204	—
Budoia	8	8	Low rise	0.0432	Complete
			Mid rise	0.0434	Complete
Sacile	7–8	7	Low rise	0.0213	Extensive
			Mid rise	0.0216	—
Polcenigo	8	8	Low rise	0.0314	Complete
			Mid rise	0.0343	Extensive
Porcia	7	6	Low rise	0.0051	—
			Mid rise	0.0056	—

This table includes the macroseismic intensity (IMS) recorded (according to Rovida *et al.*, 2021) and simulated for each municipality.

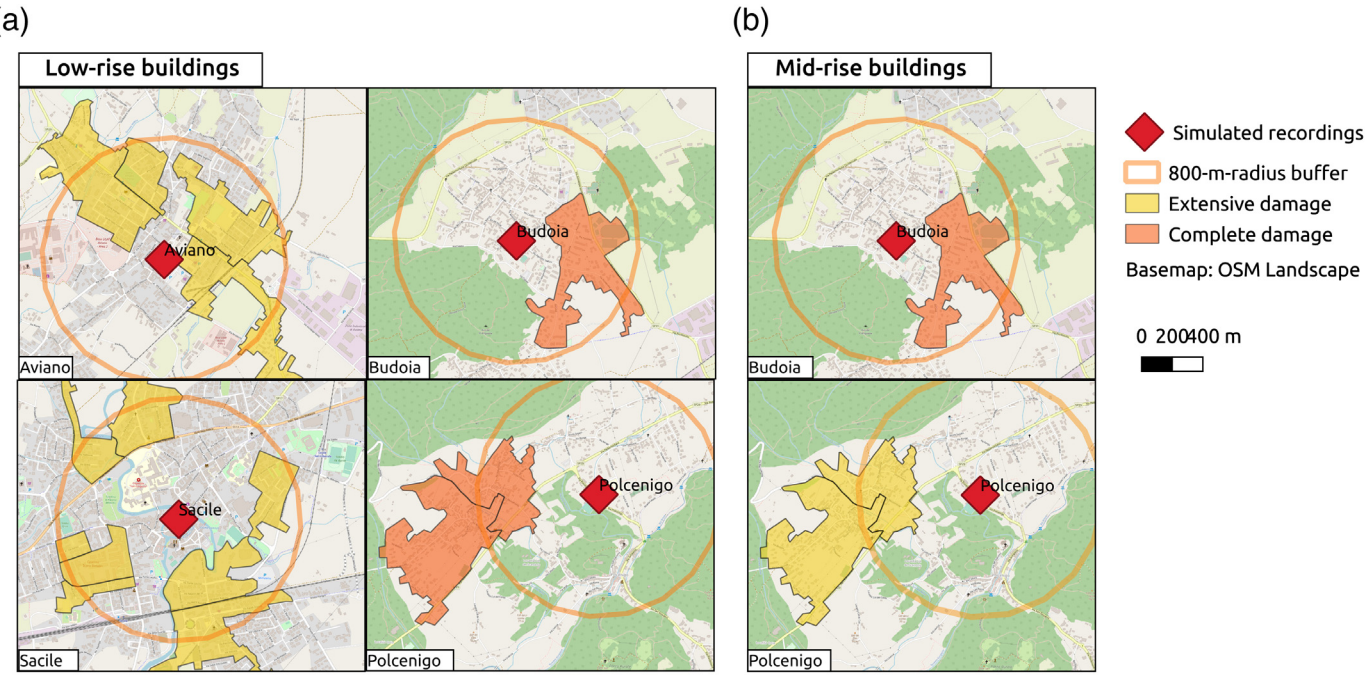

Figure 7. Maps show the location of the simulated recording, the 800 m circular area, and the damage level in the target area for the four municipalities expected to sustain structural damages (Aviano, Budoia, Polcenigo, and Sacile). The structural damage level (yellow represents extensive or orange represents complete) has been calculated for the simulated Cansiglio event. Results are shown for (a) low-rise buildings and (b) mid-rise buildings. In Aviano and Sacile, structural damage is expected only for low-rise buildings. No structural damage is expected for both low- and mid-rise buildings in Porcia. The color version of this figure is available only in the electronic edition.

may be affected by such damages. The highest structural damage level ("complete") is expected to be reached in target areas of Budoia and Polcenigo, in agreement with the recorded IMS of the 1936 event, whereas for Aviano, we expect extensive damage for low-rise buildings. The observed IMS in Sacile was 7–8, in agreement with our results that estimate an "extensive" structural damage level and a IMS of 7. However, there are some slight discrepancies between the expected damages and the IMS from the 1936 event (Table 3): in agreement with that according to our results, no structural damage is expected in Porcia, where the observed and estimated macroseismic intensities for the 1936 event are 7 and 6, respectively. This is probably due to many concurrent factors, among them the high uncertainties in the estimates of macroseismic intensities, the changes in the building stock (from historical to modern masonry), and the fact that we considered only synthetic seismograms on bedrock, disregarding the effect of soil amplification. The simulations for the Cansiglio earthquake were in fact computed on bedrock conditions because detailed amplification curves describing the local soil effects are not available. The lack of information about the local soil conditions influences the final results and may lead to underestimation of expected damages. Furthermore, our simulations consider only a simple finite-fault model with an asperity placed in the middle of the rupture area and the rupture propagating from northeast to southwest. Porcia is located at southeast of the fault, and it is influenced by the rupture propagating from the bottom to the surface along the dip plane. However, possible complex source effects (e.g., the presence of additional local asperities in the slip distribution, complexities in the propagation process) can increase the shaking observed at this site.

The results presented here are obtained under two main assumptions: (a) the dynamic response of the considered building typology can be modeled with an SDOF oscillator, and (b) the damping of 5% suggested in the literature (e.g., Eurocode 8, 2004) is valid for the considered buildings. The method successfully replicates the displacement and drift on single buildings, as shown for the M_L 3.7 event, which was recorded in Aviano by the SentiNet network. To avoid underestimation of the drift and the total displacement, we assume the lower damping factor found for the two main building directions of the SentiNet building for the building typology. Moreover, we consider the maximum displacement of the two components. If the displacement limits are exceeded, we can conservatively assess whether the damage state occurs in the target area, whereas we do not provide damage estimates for specific buildings. The method is applicable to any kind of strong-motion recordings in a target area (instrumented buildings are not required).

The use of displacement as a proxy of damage in a single monitored building had already been introduced by other authors (e.g., Spina *et al.*, 2011; Dolce *et al.*, 2017) based on

the double integration of the recordings at the building's top. Parolai *et al.* (2015) provided a simplified method that allows to estimate the acceleration at the top directly from ground-motion recordings at the bottom. Here, we enhance the method of Parolai *et al.* (2015) by calculating the displacement at the top of the building, and we extend it to a building typology representative of the residential building stock. A similar approach had been proposed for nonstructural damage assessment based on estimated ground-motion parameters (Megalooikonomou *et al.*, 2018). The method presented here, exemplified by means of a case study, can be applied using different displacement or drift limits available in the literature for specific building typologies (which may be defined for age and height classes different from the ones considered here) and can account for the recent developments related to displacement-based damage assessment (O'Reilly *et al.*, 2020).

In our study, we consider displacement thresholds from the literature as a proxy for damage. The total displacement at the top of a building is obtained as a sum of the displacement at the bottom and the relative displacement, which is simulated as that of an SDOF (or MDOF) oscillator. Depending on the frequency content of the energy of the considered event (magnitude and distance) and the dynamic characteristics of the analyzed buildings and thus of their frequencies, the contribution to the relative displacement may be greater or smaller (e.g., Vanmarcke, 1976). In the case of the considered low-rise stiff masonry buildings, the main contribution to the displacement at the top of the buildings comes from the displacement at the bottom because the fundamental frequencies of the considered building do not lie in the frequency range of the main energy contribution of the considered event (see Fig. S2 for displacement response spectra for the five sites).

The high variability found in fundamental frequencies derived from experimental data (Fig. 5) had already been explored by Michel *et al.* (2010). Such variability can have an impact on damage assessment results. Thus, further analyses should be performed to explore the variability of the experimental frequencies for the specific masonry building typology (e.g., using the shaking table to assess fundamental frequency, damping, and expected changes under seismic action; Penna *et al.*, 2016; Morandi *et al.*, 2018). In addition, the relations between soil and building frequencies (e.g., Gallipoli *et al.*, 2020) and the effect of soil–foundation–structure interaction, so far included in the fundamental period of the soil–structure system, should be accounted for. Further measurements are required to achieve a statistically representative population and to infer average and standard deviation of the fundamental frequency clusters identified for the building typology. Such analyses could also be enriched by observations of experimental period–height relationships associated to specific damage states (e.g., Ditommaso *et al.*, 2013) when available.

The definition of target areas relies on the assumption that the strong motion does not vary in the proximity of a strong-motion sensor. This step is particularly relevant to exclude ground-motion variations caused by local site effects. Thus, to define the target area, the local geological conditions should be taken into account to exclude variations of site amplifications. For the case study presented here, the soil types found at the target areas do not amplify the ground motion in the considered frequency band. However, target areas may be smaller in highly heterogeneous localities or larger in case of highly homogeneous soil conditions. Given that the sensor recordings account for site effects, the ground motion in homogeneous, and properly defined target areas are realistic inputs for the proposed method.

Conclusions

We developed a method that uses strong-motion recordings and a selected building typology to estimate the expected damage in case of a seismic event. The main novelty consists in generalizing a method usually adopted for specific buildings to a simple and common building typology that accounts for a substantial fraction of the building stock. The method presented here can support the definition of first-level risk scenarios based on historical or user-defined seismic events and contributes to increasing preparedness in case of occurrence of similar events in the future. Results can provide strong support during emergencies, in particular to emergency managers (e.g., civil protection) to plan effective life-saving response actions.

The method presented here can be extended to other areas in Italy and worldwide. Future developments should be devoted to:

- Extending the method to other regular building typologies, in particular regular RC frames. The method can also be extended to more complex building typologies, but this requires an additional effort to identify the higher modes and associate the results to the selected typology, ensuring the representativity of the typology dynamic response.
- Applying the method in areas with less data available (e.g., for areas where no digital building map or Istat census is available). The lack of data can be counterbalanced by in-person inspections or with the use of remote-sensing data.
- Enhancing the definition of target areas and accounting for ground-motion correlation and site effects to identify homogeneous areas.
- Using the method in combination with classical damage estimation methods (e.g., Silva *et al.*, 2015; Borzi *et al.*, 2019) usually applied at municipality scale, increasing the damage assessment spatial resolution in areas of interest. Future work will be devoted to enhancing the existing damage assessment described by Poggi *et al.* (2020) for FVG and Veneto, where ground-motion sensors are available (and currently growing in number).

- Complementing the method with the expert crowdsourcing performed by civil protection volunteers, who provide reports of the perceived shaking in case of occurrence of seismic events in FVG (Sandron *et al.*, 2021).

Data and Resources

Italian census data were provided by Italian National Institute of Statistics (Istat, Italy), and their use is allowed for research purposes. The digital buildings map for Friuli Venezia Giulia (FVG) was provided by the Friuli Venezia-Giulia regional government (http://www.regione.fvg.it/rafvg/cms/RAFVG/ambiente-territorio/conoscere-ambiente-territorio/FOGLIA4, last accessed October 2020). Target area maps were produced using the open-source QGIS Geographic Information System (http://qgis.org, last accessed April 2021). The recorded macroseismic intensities were extracted from the latest available version of the CPTI15 database (Parametric Catalogue of Italian Earthquakes; Rovida *et al.*, 2021). The M_L 3.7 event (http://rts.crs.inogs.it/event/68692/detail.html, last accessed May 2021) were recorded by the SentiNet sensors installed in the Aviano city hall and managed by National Institute of Oceanography and Applied Geophysics (OGS). The supplemental material for this article includes the synthetic seismograms of the 1936 Cansiglio event and the displacement response spectra for the east, north, and vertical components, at the location of the five instrumented buildings considered for the municipalities of Aviano, Budoia, Polcenigo, Porcia, and Sacile.

Declaration of Competing Interests

The authors acknowledge there are no conflicts of interest recorded.

Acknowledgments

The authors thank Editor-in-Chief A. Bent and two anonymous reviewers for their suggestions that helped improving the final article. This research was partially funded by two research projects: "Edifici sentinella" (research project financed by the local government) and ARMONIA project (real-time acceleration network for monitoring sites and buildings in Italy and Austria, 2014–2020 INTERREG V-A Italy–Austria). The authors also thank all the partners involved in the research project: Friuli Venezia Giulia (FVG) and Veneto regional Civil Protection, University of Innsbruck (AT), University of Trieste and University of Udine (IT), Zentralanstalt für Meteorologie und Geodynamik (ZAMG, AT), and the Agenzia regionale per la protezione ambientale (ARPA) of the Veneto region. Bojana Petrovic is supported by a research fellowship from the German Research Foundation (DFG, PE 2891/1-1). The authors also thank the Istat national offices (Rome) and the regional office of Friuli Venezia Giulia for providing the census data at census unit scale. The authors also thank Floriana Marino (Museum Tiere Motus, Venzone) for providing useful information on the northeastern Italy building typologies. The authors acknowledge the FVG Civil Protection personnel (in particular Gabriele Peressi and Damiano Giordani) and volunteers (in particular Claudio Pegorer and Paolo Fedrigo) and the colleagues at National Institute of Oceanography and Applied Geophysics (OGS) (in particular Carla Barnaba, Ilaria Dreossi, and Gregorio Bottaro) for their help in identifying the buildings and performing the noise measurement. The authors also thank the municipality of Aviano and in particular the urban planning department for providing all the information on the selected buildings in the target area. Finally, the authors thank all the residents that gave their permissions for the noise measurements to be performed at their domiciles. Some of the figures were drawn using Generic Mapping Tools (GMT; Wessel *et al.*, 2019).

References

Abo-El-Ezz, A., M. Nollet, and M. Nastev (2013). Seismic fragility assessment of low-rise stone masonry buildings, *Earthq. Eng. Eng. Vib.* **12,** 87–97, doi: 10.1007/s11803-013-0154-4.

Bal, I. E, H. Crowley, and R. Pinho (2008). Displacement-based earthquake loss assessment for an earthquake scenario in Istanbul, *J. Earthq. Eng.* **12** (suppl. 2), 12–22, doi: 10.1080/13632460802013388.

Bernardini, A. (2008). Vulnerability analyses in a sample of 18 municipalities in the Veneto-Friuli Area (NE Italy), *Boll. Geof. Teor. Appl.* **49,** 447–462.

Bernardini, A., L. Salmaso, and A. Solari (2008). Statistical evaluation of vulnerability and expected seismic damage of residential buildings in the Veneto-Friuli area (NE Italy), *Boll. Geof. Teor. Appl.* **49,** 427–446.

Bindi, D., B. Petrovic, S. Karapetrou, M. Manakou, T. Boxberger, D. Raptakis, K. D. Pitilakis, and S. Parolai (2015). Seismic response of an 8-story RC-building from ambient vibration analysis, *Bull. Earthq. Eng.* **13,** 2095–2120, doi: 10.1007/s10518-014-9713-y.

Borzi, B., M. Faravelli, and D. A. Polli (2019). Central Italy sequence: Simulated damage scenario for the main 2016 shocks, *Bull. Earthq. Eng.* **17,** 5559–5581, doi: 10.1007/s10518-018-0378-9.

Bragato, P. L., P. Comelli, A. Saraò, D. Zuliani, L. Moratto, V. Poggi, G. Rossi, C. Scaini, M. Sugan, C. Barnaba, *et al.* (2021). The OGS—Northeastern Italy seismic and deformation network: Current status and outlook, *Seismol. Res. Lett.* **92,** no. 3, 1704–1716, doi: 10.1785/0220200372.

CEN (2004). European standard EN 1998-1: 2004—Eurocode 8: Design of structures for earthquake resistance. Part 1: General rules, seismic action and rules for buildings, European Committee for Standardization, Brussels, Belgium.

Chourasia, A., S. K. Bhattacharyya, N. M. Bhandari, and P. Bhargava (2016). Seismic performance of different masonry buildings: Full-scale experimental study, *J. Perform. Constructed Facil.* **30,** no. 5, doi: 10.1061/(ASCE)CF.1943-5509.0000850.

Crowley, H., and R. Pinho (2004). Period-height relationship for existing European reinforced concrete buildings, *J. Earthq. Eng.* **8,** special issue no. 1, 93–119.

Crowley, H., and R. Pinho (2006). Simplified equations for estimating the period of vibration of existing buildings, *First European Conf. on Earthquake Engineering and Seismology (a Joint Event of the 13th ECEE & 30th General Assembly of the ESC)*, Geneva, Switzerland, 3–8 September 2006, Paper Number 1122.

D'Ayala, D., K. S. Jaiswal, D. J. Wald, K. Porter, and M. Greene (2010). Collaborative effort to estimate collapse fragility for buildings worldwide: The WHE-PAGER project, *Ninth U.S. National and 10th Canadian Conf. on Earthquake Engineering*, Toronto, Canada, 25–29 July 2010.

Del Gaudio, C., G. De Martino, M. Di Ludovico, G. Manfredi, A. Prota, P. Ricci, and G. M. Verderame (2017). Empirical fragility curves from damage data on RC buildings after the 2009 L'Aquila earthquake, *Bull. Earthq. Eng.* **15,** 1425–1450, doi: 10.1007/s10518-016-0026-1.

Ditommaso, R., M. Vona, M. R. Gallipoli, and M. Mucciarelli (2013). Evaluation and considerations about fundamental periods of damaged reinforced concrete buildings, *Nat. Hazards Earth Syst. Sci.* **13,** 1903–1912, doi: 10.5194/nhess-13-1903-2013.

Dolce, M., B. Borzi, D. Da Porto, M. Faravelli, S. Lagomarsino, G. Magenes, C. Moroni, A. Penna, A. Prota, E. Speranza, *et al.* (2019). Mappe di rischio sismico per il territorio italiano, *Conf.: XVIII Convegno ANIDIS "L'Ingegneria Sismica in Italia"*, Ascoli Piceno, Italy (in Italian).

Dolce, M., M. Nicoletti, A. De Sortis, S. Marchesini, D. Spina, and F. Talanas (2017). Osservatorio sismico delle strutture: The Italian structural seismic monitoring network, *Bull. Earthq. Eng.* **15,** 621–641, doi: 10.1007/s10518-015-9738-x.

Donà, M., P. Carpanese, V. Follador, L. Sbrogiò, and F. Da Porto (2020). Mechanics-based fragility curves for Italian residential URM buildings, *Bull. Earthq. Eng.* doi: 10.1007/s10518-020-00928-7.

Dunand, F., P. Guéguen, P.-Y. Bard, J. Rodgers, and M. Celebi (2006). Comparison of the dynamic parameters extracted from weak, moderate and strong building motion, *Proc. of the 1st European Conf. of Earthquake Engineering and Seismology*, Geneva, Switzerland, Paper Number 1021.

Espinosa-Aranda, J. M., A. Cuellar, A. Garcia, G. Ibarrola, R. Islas, S. Maldonado, and F. H. Rodriguez (2009). Evolution of the Mexican Seismic Alert System (SASMEX), *Seismol. Res. Lett.* **80,** no. 5, 694–706, doi: 10.1785/gssrl.80.5.694.

Farsi, M., and P.-Y. Bard (2004). Estimation des périodes propres de bâtiments et vulnérabilité du bâti existant dansl'agglomération de Grenoble, *Revue Française de Génie Civil* **8,** no. 2, 149–179 (in French).

Ferrario, V. (2009). Agropolitana. Dispersed city and agricultural spaces in Veneto region (Italy), *The 4th International Conf. of the International Forum on Urbanism (IFoU), The New Urban Question – Urbanism beyond Neo-Liberalism*, Amsterdam/Delft, 26–28 November.

Frankie, T. M., B. Gencturk, and A. S. Elnashai (2013). Simulation-based fragility relationships for unreinforced masonry buildings, *J. Struct. Eng. (U. S.)* **139,** 400–410, doi: 10.1061/(ASCE)ST.1943-541X.0000648.

Gallipoli, M. R., G. Calamita, N. Tragni, D. Pisapia, M. Lupo, M. Mucciarelli, T. Stabile, A. Perrone, L. Amato, F. Izzi, *et al.* (2020). Evaluation of soil-building resonance effect in the urban area of the city of Matera (Italy), *Eng. Geol.* **272,** 105645, doi: 10.1016/j.enggeo.2020.105645.

Gallipoli, M. R., M. Mucciarelli, B. Šket-Motnikar, P. Zupančić, A. Gosar, S. Prevolnik, M. Herak, J. Stipčević, D. Herak, Z. Milutinović, *et al.* (2010). Empirical estimates of dynamic parameters on a large set of European buildings, *Bull. Earthq. Eng.* **8,** 593–607, doi: 10.1007/s10518-009-9133-6.

Gallipoli, M. R., M. Mucciarelli, and M. Vona (2009). Empirical estimate of fundamental frequencies and damping for Italian buildings, *Earthq. Eng. Struct. Dynam.* **38,** 973–988, doi: 10.1002/eqe.878.

Goel, R. K., and A. K. Chopra (1997). Period formulas for moment-resisting frame buildings, *Struct. Eng. Div. ASCE* **123,** 1454–1461.

Gomez-Capera, A. A., M. D'Amico, G. Lanzano, M. Locati, and M. Santulin (2020). Relationships between ground motion parameters and macroseismic intensity for Italy, *Bull. Earthq. Eng.* **18,** 5143–5164, doi: 10.1007/s10518-020-00905-0.

Gorini, A., M. Nicoletti, P. Marsan, R. Bianconi, R. De Nardis, L. Filippi, S. Marcucci, F. Palma, and E. Zambonelli (2010). The Italian strong motion network, *Bull. Earthq. Eng.* **8,** 1075–1090, doi: 10.1007/s10518-009-9141-6.

Gosar, A. (2012). Determination of masonry building fundamental frequencies in five Slovenian towns by microtremor excitation and implications for seismic risk assessment (2012), *Nat. Hazards* **62,** no. 3, doi: 10.1007/s11069-012-0138-0.

Grünthal, G. (Editor) (1998) European macroseismic scale 1998 (EMS-98), in *Cahiers du Centre Européen de Géodynamique et de Séismologie*, Vol. 15, Centre Européen de Géodynamique et de Séismologie, Luxembourg, 99 pp. (in French).

Guatteri, M., P. M. Mai, and G. C. Beroza (2004). A pseudo-dynamic approximation to dynamic rupture models for strong ground motion prediction, *Bull. Seismol. Soc. Am.* **94,** 2051–2063, doi: 10.1785/0120040037.

Guidoboni, E., G. Ferrari, G. Tarabusi, G. Sgattoni, A. Comastri, D. Mariotti, C. Ciuccarelli, M. G. Bianchi, and G. Valensise (2019). CFTI5Med, the new release of the catalogue of strong earthquakes in Italy and in the Mediterranean area, *Sci. Data* **6,** 80, doi: 10.1038/s41597-019-0091-9.

Guler, K., E. Yuksel, and A. Kocak (2008). Estimation of the fundamental vibration period of existing RC buildings in Turkey utilizing ambient vibration records, *J. Earthq. Eng.* **12,** no. S2, 140–150, doi: 10.1080/13632460802013909.

Hong, L.-L., and W.-L. Hwang (2000). Empirical formula for fundamental vibration periods of reinforced concrete buildings in Taiwan, *Earthq. Eng. Struct. Dynam.* **29,** 327–337.

Istat (2011). 15° Censimento della popolazione e delle abitazioni 2011, National buildings census, Istituto Nazionale di Statistica, Rome, Italy (in Italian).

Jaiswal, K. S., and D. J. Wald (2008). Creating a global building inventory for earthquake loss assessment and risk management, *U.S. Geol. Surv. Open-File Rept. 2008-1160*, 106 pp.

Jin, X., Q. Ma, and S. Li (2004). Comparison of four numerical methods for calculating seismic dynamic response of SDOF systems, *13th World Conf. on Earthquake Engineering*, Vancouver, Canada, 1–6 August 2004, Paper Number 2889.

Lagomarsino, S., and S. Giovinazzi (2006). Macroseismic and mechanical models for the vulnerability and damage assessment of current buildings, *Bull. Earthq. Eng.* **4,** 415–443, doi: 10.1007/s10518-006-9024-z.

Lang, D. H., A. Kumar, S. Sulaymanov, and A. Meslem (2018). Building typology classification and earthquake vulnerability scale of Central and South Asian building stock, *J. Build. Eng.* **15,** 261–277, ISSN 2352-7102, doi: 10.1016/j.jobe.2017.11.022.

Lee, V. W. (1990). Efficient algorithm for computing displacement, velocity and acceleration responses of an oscillator to arbitrary ground motion, *Soil Dynam. Earthq. Eng.* **l9,** no. 6, 288–300.

Malagnini, L., A. Akinci, R. Herrmann, N. A. Pino, and L. Scognamiglio (2002). Characteristics of the ground motion in Northeastern Italy, *Bull. Seismol. Soc. Am.* **92,** 2186–2204.

Masi, A., L. Chiauzzi, G. Santarsiero, V. Manfredi, S. Biondi, E. Spacone, C. Del Gaudio, P. Ricci, G. Manfredi, and G. M. Verderame (2019). Seismic response of RC buildings during the Mw 6.0 August 24, 2016 Central Italy earthquake: The Amatrice case study, *Bull. Earthq. Eng.* **17,** 5631–5654, doi: 10.1007/s10518-017-0277-5.

Megalooikonomou, K. G., S. Parolai, and M. Pittore (2018). Toward performance-driven seismic risk monitoring for geothermal platforms: Development of ad hoc fragility curves, *Geoth. Energ.* **6,** 8, doi: 10.1186/s40517-018-0094-3.

Meroni, F., V. Pessina, and A. Bernardini (2008). Damage risk and scenarios in the Veneto - Friuli area, *Boll. Geof. Teor. Appl.* **9,** 485–503.

Michel, C., P. Gueguen, P. Lestuzzi, and P.-Y. Bard (2010). Comparison between seismic vulnerability models and experimental dynamic properties of existing buildings in France (2010), *Bull. Earthq. Eng.* **8,** 1295–1307, doi: 10.1007/s10518-010-9185-7.

Morandi, P., L. Albanesi, F. Graziotti, T. Li Piani, A. Penna, and G. Magenes (2018). Development of a dataset on the in-plane experimental response of URM piers with bricks and blocks, *Construct. Build. Mater.* **190,** 593–611, doi: 10.1016/j.conbuildmat.2018.09.070.

Moratto, L., and A. Saraò (2012). Improving ShakeMap performance by integrating real with synthetic data: Tests on the 2009 Mw = 6.3 L'Aquila Earthquake (Italy), *J. Seismol.* **16,** 131–145, doi: 10.1007/s10950-011-9253-8.

Moratto, L., P. Suhadolc, and G. Costa (2011). ShakeMaps for three relevant earthquakes in the Southeastern Alps: Comparison between instrumental and observed intensities, *Tectonophysics* **509,** 93–106.

Moratto, L., P. Suhadolc, and G. Costa (2012). Finite-fault parameters of the September 1976 M > 5 aftershocks in Friuli (NE Italy), *Tectonophysics* **536/537,** 44–60.

Moratto, L., A. Vuan, and A. Saraò (2015). A hybrid approach for broadband simulations of strong ground motion: The case of the 2008 Iwate–Miyagi Nairiku earthquake, *Bull. Seismol. Soc. Am.* **105,** 2823–2829.

Mori, J., H. Kanamori, J. Davis, E. Hauksson, E. Clayton, T. Heaton, L. Jones, A. Shakal, and R. Porcella (1998). Major improvements in progress for Southern California earthquake monitoring, *Eos Trans. AGU* **79,** 217–221.

Motazedian, D., and G. M. Atkinson (2005). Stochastic finite-fault modeling based on a dynamic corner frequency, *Bull. Seismol. Soc. Am.* **95,** 995–1010.

Mucciarelli, M., and M. R. Gallipoli (2007). Non-parametric analysis of a single seismometric recording to obtain building dynamic parameters, *Ann. Geophys.* **50,** no. 2, 259–266, doi: 10.4401/ag-3079.

Norme Tecniche per le Costruzioni (NTC) (2018). Aggiornamento delle norme tecniche per le costruzioni, *decreto ministeriale 17 gennaio 2018, GU n.35 del 11-2-2019 – Suppl. Ordinario n. 5*, available at https://www.gazzettaufficiale.it/eli/id/2018/2/20/18A00716/sg (last accessed October 2020) (in Italian).

Okada, Y., K. Kasahara, S. Hori, K. Obara, S. Sekiguchi, H. Fujiwara, and A. Yamamoto (2004). Recent progress of seismic observation networks in Japan—Hi-net, F-net, K-NET and KiK-net—, *Earth Planets Space* **56,** xv–xxviii, doi: 10.1186/BF03353076.

O'Reilly, G. J., R. Monteiro, B. N. Al Mouayed, T. J. Sullivan, and G. M. Calvi (2020). Displacement-based framework for simplified seismic loss assessment, *J. Earthq. Eng.* **24** (suppl. 1), 1–22, doi: 10.1080/13632469.2020.1730272.

Parolai, S., D. Bindi, T. Boxberger, C. Milkereit, K. Fleming, and M. Pittore (2015). On-site early warning and rapid damage forecasting using single stations: Outcomes from the REAKT project, *Seismol. Res. Lett.* **86,** no. 5, 1393–1404, doi: 10.1785/0220140205.

Parolai, S., T. Boxberger, M. Pilz, K. Fleming, M. Haas, M. Pittore, B. Petrovic, B. Moldobekov, A. Zubovich, and J. Lauterjung (2017). Assessing earthquake early warning using sparse networks in developing countries: Case study of the Kyrgyz Republic, *Front. Earth Sci.* doi: 10.3389/feart.2017.00074.

Penelis, G., A. Kappos, and K. C. Stylianidis (2003). On the seismic vulnerability of existing unreinforced masonry buildings, *J. Earthq. Eng.* 407–423, doi: 10.1080/13632460309350456.

Penna, A., I. E. Senaldi, A. Galasco, and G. Magenes (2016). Numerical simulation of shaking table tests on full-scale stone masonry buildings, *Int. J. Architect. Herit.* **10,** nos. 2/3, 146–163, doi: 10.1080/15583058.2015.1113338.

Petrovic, B., S. U. Dikmen, and S. Parolai (2018). Real data and numerical simulations-based approaches for estimating the dynamic characteristics of a tunnel formwork building, *Bull. Earthq. Eng.* **16,** 1633–1656, doi: 10.1007/s10518-017-0250-3.

Pittore, M., M. Haas, and K. G. Megalooikonomou (2018). Risk-oriented, bottom-up modeling of building portfolios with faceted taxonomies, *Front. Built Environ.* **4,** 41, doi: 10.3389/fbuil.2018.00041.

Poggi, V., C. Scaini, L. Moratto, G. Peressi, P. Comelli, P. L. Bragato, and S. Parolai (2020). Rapid damage scenario assessment for earthquake emergency management, *Seismol. Res. Lett.* doi: 10.1785/0220200245.

Polese, M., M. Gaetani, A. D'Aragona, and A. Prota (2019). Simplified approach for building inventory and seismic damage assessment at the territorial scale: An application for a town in southern Italy, *Soil Dynam. Earthq. Eng.* **121,** 405–420, doi: 10.1016/j.soildyn.2019.03.028.

Rovida, A., M. Locati, R. Camassi, B. Lolli, P. Gasperini, and A. Antonucci (2021). Catalogo Parametrico dei Terremoti Italiani (CPTI15), Versione 3.0., Istituto Nazionale di Geofisica e Vulcanologia (INGV), doi: 10.13127/CPTI/CPTI15.3 (in Italian).

Ruiz-Garcia, J., and M. Negrete (2009). A simplified drift-based assessment procedure for regular confined masonry buildings in seismic regions, *J. Earthq. Eng.* **13,** no. 4, 520–539, doi: 10.1080/13632460802598560.

Sandron, D., T. Tufaro, A. Scolobig, F. Di Bernardo, S. Parolai, and A. Rebez (2021). A citizen science approach for supporting rapid earthquake impact assessments, *Int. J. Disast. Risk Reduct.* **52,** 101969, doi: 10.1016/j.ijdrr.2020.101969.

Satriano, C., L. Elia, C. Martino, M. Lancieri, A. Zollo, and G. Iannaccone (2011). PRESTo, the earthquake early warning system for Southern Italy: Concepts, capabilities and future perspectives, *Soil Dynam. Earthq. Eng.* **31,** 137–153, doi: 10.1016/j.soildyn.2010.06.008.

Shahzada, K., A. N. Khan, A. S. Elnashai, M. Ashraf, M. Javed, A. Naseer, and B. Alam (2012). Experimental seismic performance evaluation of unreinforced brick masonry buildings, *Earthq. Spectra* **28,** no. 3, 1269–1290, doi: 10.1193/1.4000073.

Silva, V., H. Crowley, H. Varum, and R. Pinho (2015). Seismic risk assessment for mainland Portugal, *Bull. Earthq. Eng.* **13,** 429–457, doi: 10.1007/s10518-014-9630-0.

Sirovich, L., and F. Pettenati (2004). Source inversion of intensity patterns of earthquakes: A destructive shock in 1936 in Northeast Italy, *J. Geophys. Res.* **109,** no. B10309, doi: 10.1029/2003JB002919.

So, E., and R. Spence (2013). Estimating shaking-induced casualties and building damage for global earthquake events: A proposed modelling approach, *Bull. Earthq. Eng.* **11,** 347–363, doi: 10.1007/s10518-012-9373-8.

Spina, D., B. G. Lamonaca, M. Nicoletti, and M. Dolce (2011). Structural monitoring by the Italian Department of Civil Protection and the case of 2009 Abruzzo seismic sequence, *Bull. Earthq. Eng.* **9,** 325–346, doi: 10.1007/s10518-010-9232-4.

Spudich, P., and L. Xu (2003). Documentation of software package Compsyn sxv3.11: Programs for earthquake ground motion calculation using complete 1-D Green's functions, in *International Handbook of Earthquake and Engineering Seismology CD*, W. Lee, P. Jennings, C. Kisslinger, and H. Kanamori (Editors), International Association of Seismology and Physics of Earth's Interior, Academic Press, Cambridge, Massachusetts, 1200 pp.

Vanmarcke, E. H. (1976). Structural response to earthquakes, in *Seismic Risk and Engineering Decisions*, C. Lomnitz and E. Rosenblueth (Editors), Vol. 15, Developments in Geotechnical Engineering, Elsevier Publishing Company, Amsterdam, The Netherlands, 278–337.

Vona, M. (2014). Fragility curves of existing RC buildings based on specific structural performance levels, *Open J. Civ. Eng.* **4,** 120–134, doi: 10.4236/ojce.2014.42011.

Wald, D. J., P. S. Earle, T. I. Allen, K. Jaiswal, K. Porter, and M. Hearne (2008). Development of the U.S. Geological Survey's PAGER system (prompt assessment of global earthquakes for response), *Proc. of the 14th World Conf. on Earthquake Engineering*, Beijing, China, 8 pp.

Wald, D. J., P. S. Earle, K. W. Lin, V. Quitoriano, and B. C. Worden (2006). Challenges in rapid ground motion estimation for the prompt assessment of global urban earthquakes, *Bull. Earthq. Res. Inst.* **81,** 275–283.

Wald, D. J., V. Quitoriano, T. H. Heaton, H. Kanamori, C. W. Scrivner, and C. B. Worden (1999). TriNet "ShakeMaps": Rapid generation of peak ground motion and intensity maps for earthquakes in Southern California, *Earthq. Spectra* **15,** 537–555.

Wessel, P., J. F. Luis, L. Uieda, R. Scharroo, F. Wobbe, W. H. F. Smith, and D. Tian (2019). The Generic Mapping Tools Version 6, *Geochem. Geophys.* **20,** 5556–5564, doi: 10.1029/2019GC008515.

Wu, W. M., D.-Y. Chen, T.-L. Lin, C.-Y. Hsieh, T.-L. Chin, W.-Y. Chang, W.-S. Li, and S.-H. Ker (2013). A high-density seismic network for earthquake early warning in Taiwan based on low cost sensors, *Seismol. Res. Lett.* **84,** no. 6, 1048–1054, doi: 10.1785/0220130085.

Erratum

Figure 2 of the original article shows the fraction of buildings constituted by unreinforced masonry, reinforced concrete, or other material. Pie charts show unreinforced masonry in yellow and reinforced concrete in light blue. However, in the published ahead of print version, the legend colors were inverted. This version contains the corrected figure. Note that the caption and the text are unvaried.